Available online at www.sciencedirect.com
SCIENCE DIRECT
Journal of Catalysis 226 (2004) 273–282
JOURNAL OF CATALYSIS
www.elsevier.com/locate/jcat

Hydrogenation of ethylene and formaldehyde on Pt (111) and $Pt_{80}Fe_{20}$ (111): a density-functional study

Robin Hirschl, Andreas Eichler, Jürgen Hafner *

Institut für Materialphysik and Center for Computational Materials Science, Universität Wien, Sensengasse 8/12, A-1090 Wien, Austria

Received 18 February 2004; revised 6 May 2004; accepted 7 May 2004

Available online 2 July 2004

Abstract

In this paper we extend our investigations of selective hydrogenation reactions catalyzed by platinum–iron alloy surfaces from the determination of adsorption energies to the calculation of reaction pathways. Trying to elucidate the experimental fact that over $Pt_{80}Fe_{20}$ alloy surfaces α,β-unsaturated aldehydes are selectively hydrogenated to unsaturated alcohols, we determine transition states and reaction rates for the hydrogenation of ethylene and formaldehyde to ethane and methanol, respectively, over pure Pt (111) and PtFe alloy surfaces. In a previous article (R. Hirschl et al., J. Catal. 217 (2003) 354) we argued that only iron atoms in the surface layer can explain the selectivity in hydrogenation. Here we investigate the influence of surface-iron atoms on energy barriers for hydrogenation. While Pt (111) and platinum-covered $Pt_{80}Fe_{20}$ (111) surfaces behave in a similar way, apart from reduced adsorption energies on the alloy surface, iron atoms in the surface have significant effects for the hydrogenation of formaldehyde. Although the reaction barrier is higher, the ratio of the energy barrier to the adsorption energy is much lower. Top-layer iron atoms do not change the behavior of the surface regarding the hydrogenation of ethylene.

Keywords: Heterogeneous catalysis; Hydrogenation; Selectivity; Ethylene; Formaldehyde; Bimetallic catalysts; Density functional theory; Transition-state theory; Reaction rates

1. Introduction

Computational heterogeneous catalysis almost inevitably lags behind experiments due to the complexity of the underlying processes. However, according to Moore's Law [1], the computational power available at a particular price rises exponentially. This brought the class of catalytic reactions that can be treated from *first principles* closer to the "real world" in several respects. With the possibility of using large calculational supercells in plane-wave-based density-functional theory (DFT) calculations (where the computational effort scales essentially as $O(N_e)^2$, with N_e the number of electrons in the system), both the description of the substrates and the adsorbates can be improved. On the one hand, we are capable of simulating alloy catalysts, which may have properties vastly different from those of their constituents, and on the other hand, reactants with, e.g., more than one reducible function, become tractable. Furthermore, we are not any more restricted to local minima in the potential energy surface (i.e., initial and final states), but can explore reaction pathways, transition states, and eventually calculate reaction rates.

In this paper we discuss energy barriers and reaction rates for the hydrogenation of C=O and C=C double bonds on close-packed Pt and Fe-alloyed Pt surfaces. It has been known for more than a decade that the addition of an electropositive metal to monometallic catalysts such as Pt changes the selectivity in the hydrogenation of α,β-unsaturated aldehydes toward unsaturated (allylic) alcohols [2–8]. Unsaturated alcohols are important intermediates in the fine chemistry industry. This class of unsaturated aldehydes, the simplest of them being acrolein (2-propenal, CH_2=CH–CH=O), presents two adjacent double bonds in conjugation. Because of thermodynamic and kinetic reasons the selective hydrogenation of the C=O double bond only is difficult to achieve on conventional hydrogenation catalysts (Pt, Ru, Ni, ...) [9].

* Corresponding author.
E-mail address: juergen.hafner@univie.ac.at (J. Hafner).

0021-9517/$ – see front matter
doi:10.1016/j.jcat.2004.05.012

Assuming a Horiuti–Polanyi mechanism [10], the hydrogenation of either double bond is preceded by the adsorption of the aldehyde via this particular bond. In a previous paper we have discussed the different adsorption modes of simple unsaturated aldehydes on $Pt_{80}Fe_{20}$ (111) alloy surfaces and their relative stability [11]. Following experimental results [12], the initial surface model consisted of a platinum-covered Pt_3Fe bulk alloy. The possibility of forming very strong Fe–O bonds, however, is capable of changing the segregation profile, bringing Fe atoms to the surface under catalytic conditions in agreement with experiments on similar systems [11]. Therefore, regarding the reactivity of the surface we have to treat segregated purely platinum-covered alloy surfaces as well as surfaces displaying Fe atoms in the surface.

We now extend this previous study to the investigation of the reaction dynamics of C=C and C=O double bond hydrogenation on model surfaces. To go straightforward to the selective hydrogenation of the unsaturated higher aldehydes is a challenging approach. To facilitate our task, we begin by studying the hydrogenation of ethylene (where only C=C bonds exist) and formaldehyde (with a C=O double bond). This is an important step in preparing the analysis of competing hydrogenations of the conjugated C=O and C=C double bonds in the unsaturated aldehydes.

The hydrogenation of olefins over metal catalysts has been one of the most studied chemical processes ever since its discovery by Sabatier and Sendersen in 1897. The chemistry of ethylene on Pt (111) has received particular attention from the surface science community as a representative case of these reactions. Recent publications on that issue report experimental results [13–15] as well as calculations [16,17]. This seemingly simple system is complicated by the fact that there appear to be at least two types of molecular adsorption states competing at higher coverages, namely a di-σ and a π bonding. Furthermore, several reaction pathways might be followed, including the hydrogenation to ethane and the conversion to ethylidyne. All these features of ethylene on Pt (111), well investigated although not yet fully understood, have been neglected in our study. Starting from a di-σ adsorption mode we adopt a Horiuti–Polanyi mechanism to successively hydrogenate ethylene via ethyl to ethane.

The hydrogenation of formaldehyde has been much less studied due its industrial insignificance. The potential product, methanol, is commonly synthesized by reducing CO or CO_2. The only work on the hydrogenation of formaldehyde known to us is a trend analysis of group VIII metals as catalysts and the effect of supports and promoters by Aika et al. [18]. In our context it is interesting to note in their result that the selectivity for methanol (in comparison to CO) correlates highly with the heat of formation of the metal oxide. The more thoroughly investigated reaction is the inverse process, the dehydrogenation of methanol, being the primary source of formaldehyde. An extensive DFT study of the dehydrogenation of methanol over Pt (111) was recently published by Desai et al. [19], using the same plane-wave-based code but other potentials.

Our paper is organized as follows: In Section 2 we list the key features of our calculations. Section 3 introduces the surface models used in our investigations. The chemisorption energies of reactants, intermediates, and products are discussed in Section 4. Energy barriers obtained from the nudged elastic band method (NEB) and reaction rates from harmonic transition-state theory (hTST) are the topic of Section 5. The concluding Section 6 summarizes our results in the context of our previous work on transition-metal alloy surfaces.

2. Methodology

Ground-state energies including ionic relaxations have been calculated within the framework of spin-polarized density-functional theory using the plane-wave-based Vienna Ab Initio Simulation Package (VASP) [20–23]. The Perdew and Wang (PW91) generalized gradient approximation (GGA) [24], adding semilocal information to the local density approximation, was used as the exchange-correlation functional. Brillouin-zone integration is performed on special grids as proposed by Monkhorst and Pack [25] utilizing a generalized Gaussian smearing. Electron–ion interactions are described using projector-augmented wave potentials [26,27]. The oxygen and carbon potentials require the plane-wave energy cutoff to be set to 400 eV.

The k-point sampling was performed using $(4 \times 4 \times 1)$ and $(3 \times 3 \times 1)$ Γ-centered grids for the (2×2) and $(2\sqrt{3} \times 2\sqrt{3})$ supercells. The number of k points was confirmed to guarantee a sufficient accuracy of the total ground-state energy [11]. In the case of $(4 \times 4 \times 1)$ k-point grids for the (2×2) cell, leading to 10 k points in the irreducible part of the Brillouin-zone, a note of caution is to be issued. While this number is generally sufficient for nonmagnetic calculations, spin-polarized systems often require a higher accuracy. However, the task of determining more than 20 reaction pathways necessitates a calculational speed up at a tolerable loss of precision. Tests on several adsorption energies and energy barriers indicated that our errors with respect to full k-point convergence are well below 10 to 15%.

The finding of transition states requires the determination of minimum energy pathways (MEP) for the reaction under investigation, the transition state being a saddle point along such a pathway. The nudged elastic band method [28,29] was applied to scan potential energy surfaces for minimum energy pathways. An initial guess with four to five images between initial and final states was continuously refined around the prospective saddle point until the distances between the images in phase space were small enough to apply the climbing image NEB [30].

After the transition state is localized, reaction rates can be estimated in the framework of harmonic transition-state theory [31]. Vibrational frequencies are obtained through fi-

nite differences of the forces to approximate the dynamical matrix. The vibrational spectra of initial and transition state allow calculation of the prefactor for the reaction rate constant [31,32].

3. Surface models

Periodic boundary conditions, as used in our calculations, lead to a slab geometry as the natural choice for the supercell setup. For close-packed surfaces such as fcc (111), four layers are sufficient to simulate a surface. Adsorption and surface segregation in the case of the alloy surface are allowed on one side of the slab only. The periodic slabs are separated by 4 layers of vacuum. A (2×2) supercell leads to an adsorbate coverage of $\Theta = \frac{1}{4}$ for ethylene and formaldehyde hydrogenation.

In Fig. 1 we have depicted the surface models used in our study. Fig. 1a shows a simple Pt (111) surface. $Pt_{80}Fe_{20}$ (111) surfaces have been well studied experimentally [12,33,34], all results agreeing on the fact that Pt strongly segregates toward the surface, leading to a continuously decreasing concentration profile of Fe toward the surface. This is also in agreement with theoretical determinations of the Pt–Fe segregation energy by Ruban et al. [35]. Consequently the initial surface model consists of a Pt_3Fe bulk covered by a single layer of pure Pt (Fig. 1b), leading to two inequivalent Pt sites in the surface layer, one with a nearest iron neighbor (Pt_1), the other without neighboring iron (Pt_2).

In a third surface model we have interchanged the subsurface iron atom with a surface Pt atom (Fig. 1c). This surface will from now on be dubbed "modified $Pt_{80}Fe_{20}$" surface. The choice of this surface model is motivated by the fact that α, β-unsaturated aldehydes very favorably adsorb on the $Pt_{80}Fe_{20}$ alloy surface via the formation of O–Fe bonds. This can be achieved on one hand through a few iron atoms backdiffusing to the surface, the driving force for the reversal of segregation being the strong difference in the adsorption via Pt and Fe atoms [11]. In a recent study we have discussed the local electronic structure and chemical activity of this modified alloy surface in great detail [36].

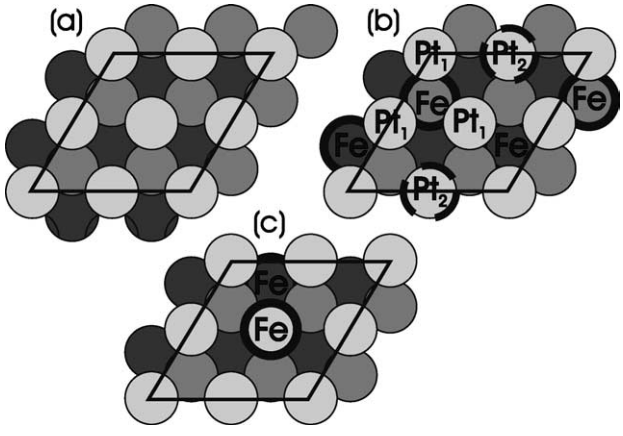

Fig. 1. (2×2) supercells of the different model surfaces: pure Pt (111) (a), platinum-covered $Pt_{80}Fe_{20}$ (111) (b), and modified $Pt_{80}Fe_{20}$ (c), showing iron atoms in the surface layer. All unlabeled atoms are Pt; for further details see the text.

4. Chemisorption energies

In this section we examine the chemisorption of the different surface species produced during the hydrogenation of ethylene and formaldehyde to ethane and methanol, respectively. Adsorption geometries are discussed, particularly regarding the C–C and C–O bond lengths, which are a measure of the strength of that bond.

In Fig. 2 we have summarized the reaction schemes. Ethylene hydrogenates via ethyl to ethane. For the hydrogenation of formaldehyde, two intermediates are possible: hydroxymethyl by adding the first hydrogen to the oxygen atom of the C=O double bond, and methoxy, by adding the first hydrogen to the carbon atom. The second hydrogenation step leads to methanol in both cases.

Adsorption energies on the three surfaces introduced in Section 3 are compiled in Table 1. For ethylene and formaldehyde two adsorption modes are considered, di-σ and π. In the former both atoms of the double bond interact with different surface atoms, in a π configuration the π system of the double bond interacts with a single surface atom. Using sum frequency generation (SFG) techniques at higher pressures, it was recently shown by Cremer and co-workers [14] that π-bound ethylene is likely to be the precursor for hydrogenation on Pt (111). This fact was corroborated theoretically by Neurock et al. [16], through calculations of ethylene hydrogenation on Pd (111). Pd surfaces do in many respects behave very similar to Pt surfaces, differences will

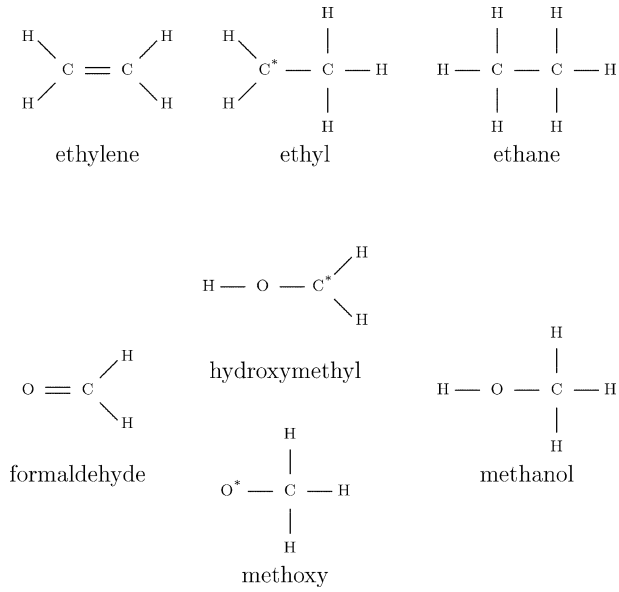

Fig. 2. Stepwise hydrogenation of ethylene to ethane (top row) and formaldehyde to methanol (bottom row).

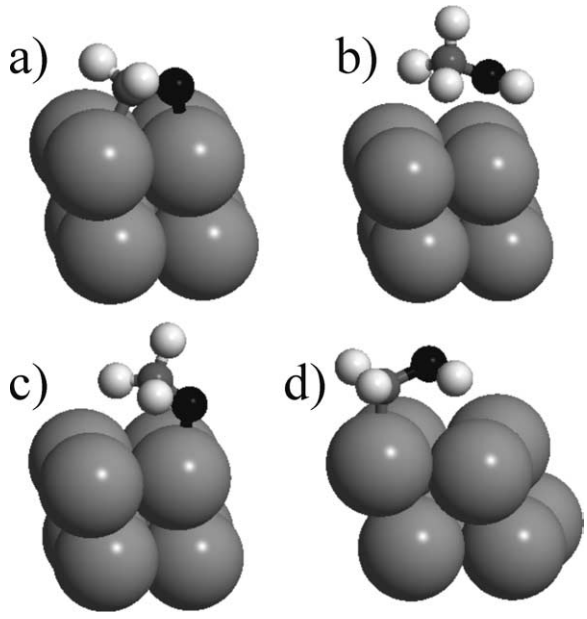

Fig. 3. Adsorption modes of formaldehyde (di-σ) (a), methanol (b), methoxy (c), and hydroxymethyl (d) on Pt (111). Adsorption geometries on the alloy surface are analogous; on the modified alloy the oxygen atom interacts with the surface iron for adsorbate species (a to c). Black, oxygen; dark gray, carbon; light gray, hydrogen.

be accentuated below. The π-ethylene species is also experimentally considered to be the reactive intermediate on other metal surfaces [37], such as Pd [38]. However, we consider only hydrogenation starting from a di-σ-adsorbed ethylene since the most favored adsorption geometries of the unsaturated aldehydes all include the C=C double bond in di-σ configuration [11].

Before we discuss the adsorption energies in detail we want to note a difference between adsorption of the intermediates on Pt (111) and Pd (111). In Fig. 3 we sketch the adsorption geometries of formaldehyde, methanol, and the hydrogenation intermediates on Pt (111). The methoxy intermediate (Fig. 3c) is found to be most stable on-top adsorbed with the C–O bond tilted with respect to the surface normal. On Pd (111) the methoxy species adsorbs in a threefold hollow site in an upright configuration with the oxygen atom pointing toward the surface, a geometry that, on Pt (111), is 110 meV less stable. Desai et al. [19] found a configuration similar to the one we present here but with the oxygen atom being in a bridge position instead of top to be the most stable adsorption mode for methoxy on Pt (111). However, their adsorption energies differ by less than 2%, and our primary issue, the comparison of pure Pt with PtFe alloy surfaces, is not affected by that discrepancy.

Coming now to adsorption energies, the first thing to note is the reduction of the adsorption energies on the platinum-covered alloy surface. The two distinct Pt sites on this surface as well as the two different species in the surface layer in the modified surface multiply the number of possible adsorption geometries. In Table 1 we have only listed the most favorable adsorption energies. The corresponding adsorption geometries show the following characteristics where applicable: (a) Oxygen atoms always bind to surface iron atoms. (b) Carbon atoms avoid surface iron atoms. (c) Pt_2 sites are more reactive than Pt_1 sites, particularly toward carbon. Consequently, one carbon atom always tries to bind to a Pt_2 atom. These properties of the $Pt_{80}Fe_{20}$ surfaces, as well as the overall reduced adsorption energies, agree with previous results on that surface alloy [11,36].

Ethylene adsorbs, as noted before, in two configurations, di-σ and π, separated in energy by 0.3–0.5 eV. The C=C axis is in both cases parallel to the surface; the hydrogen atoms are slightly tilted away from the surface. The calculated C=C bond length in gaseous ethylene is 1.32 Å. It elongates by 13% to 1.49 Å for di-σ-adsorbed ethylene on Pt and by 7% to 1.41 Å when the molecule is π adsorbed. The bond-length increase is similar on the alloy surface despite of the lower adsorption energy. The ethyl radical has an adsorption energy about twice that of ethylene. Similar to hydroxymethyl (Fig. 3d) it is adsorbed on top through the carbon atom with the methyl group canted away from the surface. The ethane molecule adsorbs with its C–C axis parallel to the surface. The hydrogen atoms are arranged in a staggered configuration as in the gas phase. Being a saturated hydrocarbon, the primary interaction force ought to be of van der Waals type, a phenomenon only poorly described by DFT. The calculated adsorption energies, being around 50 meV, are therefore certainly underestimated. The C–C bond length in the gas phase (1.53 Å) is not changed upon adsorption.

Formaldehyde adsorbs, analogous to ethylene, with its molecular axis (being C=O in this case) parallel to the surface. The lower adsorption energy with respect to ethylene causes the π configuration to be unstable. The adsorption energy of formaldehyde on Pt (111) was experimentally estimated by Abbas and co-workers [39] to be 0.54 eV, in quite good agreement with our calculated result. The relative elongation of the C=O bond upon di-σ adsorption for formaldehyde is comparable to the elongation of the C=C double bond in ethylene, i.e., by 12% from 1.21 Å in the gas phase to 1.36 Å when adsorbed. If iron atoms are present in the surface, the adsorption energy of formaldehyde almost doubles to 0.93 eV due to the formation of a very strong O–Fe bond. Interestingly, judging from the bond lengths, this does not further weaken the C=O bond; the bond is still 1.36 Å long. Furthermore, the probability that the molecule is decomposed to CH_2 and O individually adsorbed on the surface seems to be very low. The dissociation is endothermic by 0.7 eV, comparing just initial and final states. In contrast, on pure Fe (110), there is an energy gain of 0.45 eV when formaldehyde is decomposed on the surface.

The two intermediates hydroxymethyl and methoxy are again radicals and are therefore strongly adsorbed. In both cases our calculations predict a top geometry for hydroxymethyl with the coordinatively unsaturated carbon atom

Table 1
Molecular adsorption energies on Pt (111), $Pt_{80}Fe_{20}$ (111), and modified $Pt_{80}Fe_{20}$ (111) (cf. Fig. 2)

Adsorbate		Mode	Pt (111) (eV)	$Pt_{80}Fe_{20}$ (111) (eV)	Mod. $Pt_{80}Fe_{20}$ (111) (eV)
Ethylene	C_2H_4	di-σ	1.051	0.931	1.190
Ethylene	C_2H_4	π	0.678	0.637	0.696
Ethyl	C_2H_5	Top	1.950	2.006	2.065
Ethane	C_2H_6	Top	0.052	0.053	0.062
Formaldehyde	CH_2O	di-σ	0.456	0.465	**0.930**
Formaldehyde	CH_2O	π	0.017	−0.004	**0.459**
Hydroxymethyl	CH_2OH	Top	2.095	2.137	2.207
Methoxy	CH_3O	Top	1.638	1.478	**2.180**
Methanol	CH_3OH	Top	0.201	0.146	**0.513**

Results printed in boldface highlight a pronounced increase of the adsorption strength on the modified compared to the segregated alloy surfaces.

pointing toward the surface; for methoxy the undercoordinated oxygen atom binds to the substrate. For both species the C–O axis is oriented in an acute angle to the surface. Hydroxymethyl is the stronger bound species. The influence of surface iron atoms is larger in the case of methoxy, again due to a strong oxygen–iron interaction. Methanol is also top-adsorbed via the molecule's oxygen atom (Fig. 3). The molecule is saturated, but its partially polar character and high polarizability lead to a better DFT description of chemisorption than for the nonpolar ethane. From temperature-programmed desorption (TPD) experiments by Villegas et al., the adsorption energy of methanol over Pt was estimated to be 0.48 eV [40]. Our calculations underestimate this value.

All our adsorption energies of formaldehyde-derived species on Pt (111) agree accurately with previous calculations by Desai et al. [19] with the exception of the chemisorption energy of methanol, caused by a slightly inconsistent calculational setup in the previous work [41].

While for all the hydrocarbon species the adsorption energies on pure Pt, on the segregated Pt–Fe alloy surface, and on the modified Pt–Fe alloy surface are all of the same order of magnitude, formaldehyde, methanol, and their reaction intermediates (with the exception of hydroxymethyl) adsorb much more strongly on the modified alloy surface via the exposed Fe atom. The difference in the adsorption energies relative to the segregated surface varies between 0.36 eV (methanol) and 0.70 eV (methoxy). As demonstrated in our previous work [11], this difference is large enough to drive the reversal of the segregation process.

5. Reaction dynamics

Having determined the equilibrium geometries and ground-state energies of reactants, intermediates, and products in the hydrogenation processes, we will now advance one step further and investigate reaction pathways and transition states. For the hydrogenation of ethylene to ethane, it was concluded from experiments [14] and calculations [16] that the reaction occurs after a π adsorption of ethylene. Earlier experimental studies [42] reported reaction barriers of 0.65 and 0.25 eV for the first and second hydrogenation steps of ethylene over Pt (111), respectively, and assume a di-σ adsorption mode of the reactant. For the hydrogenation of formaldehyde over Pt (111) no experimental data are available.

5.1. Pathways and barriers

The reaction barriers for the hydrogenation of ethylene as well as the hydrogenation of formaldehyde via methoxy and hydroxymethyl on our three model surfaces (Secyion 3) have been determined employing the nudged elastic band method. Following the optimal adsorption position of hydrogen on Pt (111) [36], we started from a hydrogen atom adsorbed in a fcc hollow site neighboring the molecule to be hydrogenated. Only one pathway was explored per reaction; hence, we cannot claim to have found the overall optimal pathway in all cases.

The energy profiles are collected in Figs. 4–6; relevant energies are compiled in Table 2. The first two steps consist of the dissociative adsorption of hydrogen and the molecular adsorption of ethylene or formaldehyde at larger separations such that lateral interactions are negligible. This is followed by the diffusion of hydrogen toward the molecule to be hydrogenated.

Every hydrogenation process consists of two steps. After a hydrogen molecule is initially assumed to be dissociatively adsorbed somewhere far away from the molecule to be hydrogenated, a dissociated atom has to approach this mole-

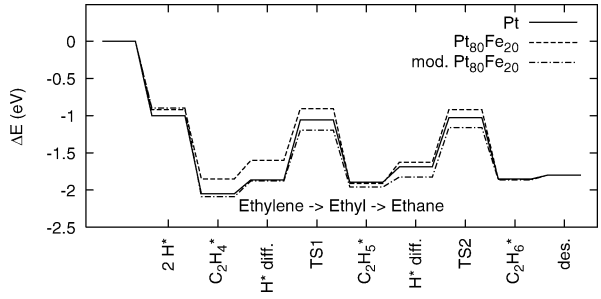

Fig. 4. Energetic profile of the hydrogenation of ethylene to ethane on different surfaces.

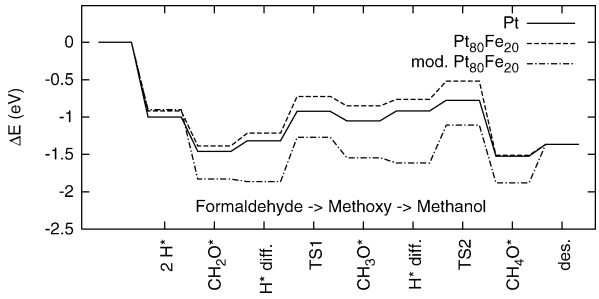

Fig. 5. Energetic profile of the hydrogenation of formaldehyde to methanol via a methoxy intermediate on different surfaces.

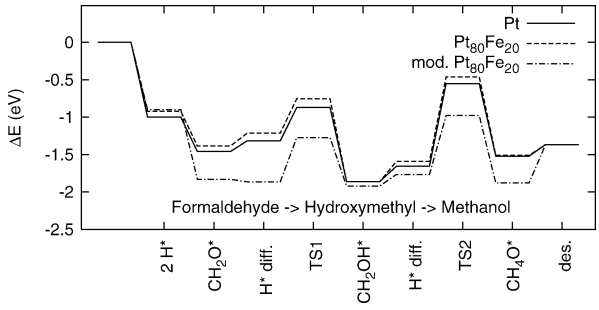

Fig. 6. Energetic profile of the hydrogenation of formaldehyde to methanol via a hydroxymethyl intermediate on different surfaces.

cule. We did not calculate diffusion barriers for hydrogen, but know from previous calculations [36] and experiments [43] that they are around 70 meV on pure Pt (111) and even lower on the PtFe alloy. Only the overall reaction energy of the hydrogen diffusion is determined. This reaction energy is generally endothermic because of the Pauli repulsion.

For the hydrogenation of ethylene to ethane on Pt (111) the first hydrogenation is the rate-determining step, having a reaction barrier 140 meV higher than the second hydrogenation step. Our barrier agrees reasonably well with previous results [16]. On the alloy surfaces the intermediate ethyl is slightly more strongly bound than on Pt (111). It interacts with only a single surface atom of type Pt_2 which is hardly influenced by iron. Consequently, while the reaction barrier for the first hydrogenation step is lower on the alloy than on the pure Pt surface, the second step has an almost identical barrier on all surfaces. The energy needed to approach the hydrogen atom to the C=C bond is in the range of 150 to 250 meV in all cases. Despite the small differences noted above, we can conclude that all three model surfaces behave similarly regarding the hydrogenation of ethylene.

Coming now to the hydrogenation of formaldehyde, there are two possible intermediates depending on whether the C–H or the O–H is the first bond to be formed. Treating first the hydrogenation via the methoxy intermediate, we again identify the first hydrogenation as the reaction step having the higher barrier. The energy barrier for the C–H bond formation in formaldehyde is much lower than in ethylene. Still, in contrast to ethylene, the total barrier (including the hydrogen diffusion) is for, the pure Pt and the Pt-covered alloy, higher than the formaldehyde adsorption energy. The overall process of C–H bond formation in formaldehyde is endothermic; in return the barrier for the second hydrogenation is very low as long as no O–Fe bond is present. The energy needed for hydrogen diffusion toward the organic molecule on the platinum-covered surfaces is slightly lower than in the case of ethylene but still between 90 and 170 meV.

Iron atoms in the surface have a major impact on the energetics of the process. The energy barrier for the first hydrogenation is higher than on the platinum-covered surfaces, but due to the high adsorption energy of formaldehyde the total barrier is 370 meV lower than the chemisorption energy. The barrier to form the O–H bond (second hydrogenation) is also around 500 meV since the strong O–Fe bond has to be broken. A very important point, however, is the energy gain when the reactant and hydrogen are coadsorbed near a surface iron atom with respect to the sum of their individual chemisorption energies. Not only is the C=O double bond bound very strongly to the substrate in the case of iron atoms in the top layer, but also the diffusion of hydrogen toward the reactant is an exothermic reaction, a substantial step in the hydrogenation of the bond.

The second reaction pathway to hydrogenate formaldehyde is via hydroxymethyl (see Fig. 6 for the energetic

Table 2
Heat of reaction ΔE_{diff} for the diffusion of atomic hydrogen toward the reactant and activation energies ΔE_{act} for the hydrogenation of formaldehyde and ethylene over pure Pt and PtFe alloy surfaces

Path	Surface	$\Delta E^{(1)}_{\text{diff}}$ (meV)	$\Delta E^{(1)}_{\text{act}}$ (meV)	$\Delta E^{(2)}_{\text{diff}}$ (meV)	$\Delta E^{(2)}_{\text{act}}$ (meV)
$C_2H_4 \rightarrow C_2H_6$	Pt	188	803	205	660
$C_2H_4 \rightarrow C_2H_6$	$Pt_{80}Fe_{20}$	250	695	285	706
$C_2H_4 \rightarrow C_2H_6$	Mod. $Pt_{80}Fe_{20}$	211	681	134	660
$CH_2O \rightarrow CH_3O \rightarrow CH_3OH$	Pt	144	391	134	142
$CH_2O \rightarrow CH_3O \rightarrow CH_3OH$	$Pt_{80}Fe_{20}$	171	491	88	243
$CH_2O \rightarrow CH_3O \rightarrow CH_3OH$	Mod. $Pt_{80}Fe_{20}$	**−34**	594	**−72**	506
$CH_2O \rightarrow CH_2OH \rightarrow CH_3OH$	Pt	144	444	203	1104
$CH_2O \rightarrow CH_2OH \rightarrow CH_3OH$	$Pt_{80}Fe_{20}$	171	461	269	1131
$CH_2O \rightarrow CH_2OH \rightarrow CH_3OH$	Mod. $Pt_{80}Fe_{20}$	**−34**	592	155	787

Cf. Fig. 6 for the complete energetic profile of the reactions. Indices 1 and 2 refer to the first and second hydrogenation steps. The species to be hydrogenated are initially adsorbed in a di-σ mode. Exothermic diffusion reactions are highlighted by boldface print.

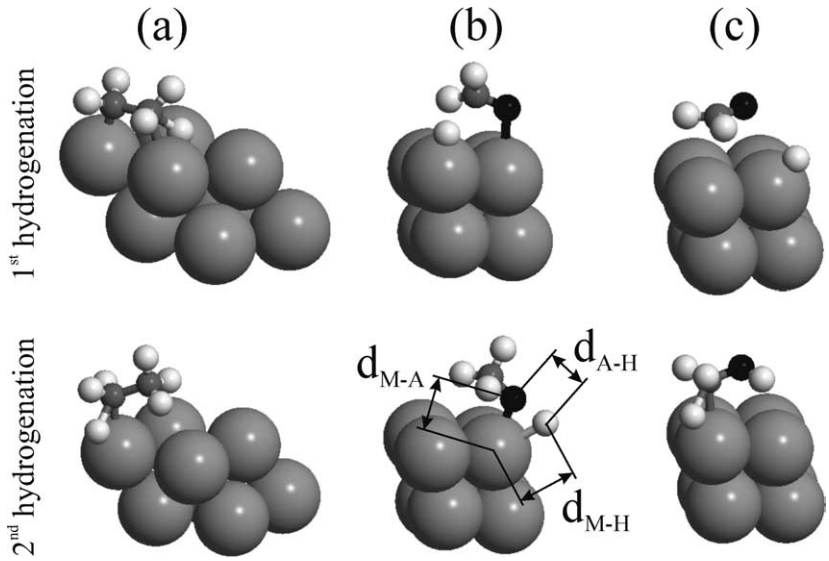

Fig. 7. Transition states over Pt (111) surfaces for the hydrogenation of ethylene (a), formaldehyde via methoxy (b), and formaldehyde via hydroxymethyl (c). Distances as given in Table 3 are indicated.

profile). Reaction barriers for the first hydrogenation (i.e., formation of the O–H) bond are very similar to the methoxy case. The second step, however, costs more than 1 eV on the platinum-covered surfaces and still 940 meV on the modified alloy surface. Not only is hydroxymethyl already in the gas phase more stable than methoxy by 350 meV, it is also much stronger bound to the substrate. Scission of the C–Pt bond and formation of a C–H bond are therefore very expensive energy-wise. An exothermic diffusion of hydrogen toward the double bond can only be observed when approaching an oxygen–iron bond. Although the first hydrogenation step is equally likely to lead to methoxy or hydroxymethyl, the full hydrogenation is only feasible via the methoxy route.

5.2. Transition states

We now discuss the transition states in more detail. Transition states for all six hydrogenation steps studied are depicted in Fig. 7 on the pure Pt (111) surface. On the alloy surfaces the transition states have a similar geometry; particular atomic distances for all transition states are compiled in Table 3.

At this point it must be noted that in a strict sense harmonic transition-state theory is not applicable to our system, since the reaction pathway often has more than one local maximum. From a threefold hollow site next to the bond to be hydrogenated the hydrogen atom in many cases first diffuses further, surmounting a first local maximum and crossing a local minimum before the actual insertion into the C=C or C=O bond occurs. The first local maximum is, however, generally lower than the second one which corresponds to the transition states shown in Fig. 7. Only for methoxy hydrogenation on the platinum-covered alloy surface the highest barrier is reached when the hydrogen atom is on top a neighboring Pt atom; consequently, the corresponding transition-state distances in Table 3 do not fit into the series.

Hydrogen–carbon bond lengths in all molecules investigated, in the gas phase as well as adsorbed, are around 1.1 Å. Hydrogen–oxygen bonds are a little shorter, around 0.97 to 1.0 Å. Transition states have C–H or O–H distances between 1.5 and 2.5 Å. Metal–carbon (or metal–oxygen) distances in transition states are between 2.3 and 3.1 Å; in the adsorbed species these distances are between 2.0 and 2.1 Å with the exceptions of methanol ($d_{\mathrm{O–M}} \approx 3.0$ Å) and ethane ($d_{\mathrm{C–M}} \approx 3.7$ Å). Furthermore, we note the following: For the hydrogenation of ethylene as well as for the hydrogenation of hydroxymethyl the transition-state geometries on the three model surfaces are very similar. In these cases no significant interaction of oxygen with the surface is involved (methanol is bound to the surface only weakly). In the other hydrogenation steps transition-state geometries differ considerably between the different surfaces. This once more indicates that alloying platinum with iron influences the hydrogenation of C=O double bonds rather than that of C=C double bonds.

5.3. Reaction rates

The last section on the reaction dynamics of the hydrogenation of formaldehyde and ethylene deals with reaction rates. For each step, the reaction rate constant k is given with hTST by

$$k = \nu \cdot \mathrm{e}^{-\Delta E_{\mathrm{act,zp}}/(k_{\mathrm{B}}T)}.$$

$\Delta E_{\mathrm{act,zp}}$ is the activation energy corrected for zero-point vibrations, and the prefactor ν is calculated in terms of the vibrational partition functions of the initial (f_{ini}) and of the

Table 3
Transition-state geometries

Path	Pt (111)			$Pt_{80}Fe_{20}$ (111)			Mod. $Pt_{80}Fe_{20}$ (111)		
	A–M	H–M	A–H	A–M	H–M	A–H	A–M	H–M	A–H
$C_2H_4 \rightarrow C_2H_5$	2.34	1.65	1.51	2.35	1.61	1.58	2.32	1.68	1.49
$C_2H_5 \rightarrow C_2H_6$	2.30	1.68	1.48	2.43	1.69	1.58	2.29	1.64	1.51
$CH_2O \rightarrow CH_3O$	3.14	1.58	2.39	2.94	1.68	1.46	3.14	1.58	2.41
$CH_3O \rightarrow CH_3OH$	2.09	2.38	1.57	2.04	2.91	2.58*	1.92	2.24	1.49
$CH_2O \rightarrow CH_2OH$	3.26	1.60	2.60	3.09	1.71	1.61	2.02	2.07	1.42
$CH_2OH \rightarrow CH_3OH$	2.54	1.70	1.46	2.49	1.67	1.46	2.31	1.65	1.45

A is the atom to be hydrogenated (carbon or oxygen), H the hydrogen atom (cf. Fig. 7). All distances in Å.
* In this reaction path the transition state is the hydrogen atom adsorbed on top of a neighboring Pt atom. From there on no further barrier exists.

transition states (f_{TS}),

$$\nu = \frac{k_B T}{h} \frac{f_{TS}}{f_{ini}}.$$

Hence, knowledge of the vibrational spectra of the initial and the transition states is required. To correctly obtain a vibrational spectrum of a transition state that contains only one imaginary eigenfrequency, the transition state mast be known with high accuracy. This can be achieved by using the "climbing image" NEB [30]. The prefactor also depends on the displacement of the atoms in determining the dynamical matrix, especially if there is a certain degree of anharmonicity. It turned out that, leaving everything else but the amplitude of the atomic displacement unchanged, the resulting prefactor could be varied by a factor of up to 4. This is because an average change in the frequencies by only 7% already leads in the case of ethane (24 frequencies) to a change of the prefactor by a factor of 5. Determining all eigenvalues of a dynamical matrix whose eigenvalue spectrum covers several orders of magnitude exactly requires forbiddingly high accuracy in the calculations. However, a factor 5 in the prefactor changes the logarithm of the rate constant only by 0.7 unit. Still the results presented in this section should be taken qualitatively rather than quantitatively.

Figs. 8–10 show the variation of the reaction rates with temperature for all hydrogenation steps investigated. Table 4 lists the zero-point-corrected activation energies.

We see in the first of the figures that in the hydrogenation of ethylene all rate constants are similar at all temperatures. On the pure Pt (111) surface the first hydrogenation is unambiguously the rate-determining step while this is not as clearly the case on the alloy surfaces. In hydrogenating formaldehyde via methoxy to methanol on platinum-covered surfaces, the first hydrogenation step is the more difficult, although only at temperatures below 450 K. For higher temperatures the second hydrogenation becomes the rate-determining step because of the low prefactor, first on Pt (111), after further heating also on $Pt_{80}Fe_{20}$. The reaction rates for the two hydrogenation steps on the modified surface are similar, but the second hydrogenation becomes more favorable only below about 250 K. Finally, in the hydrogenation of formaldehyde via hydroxymethyl the second hydrogenation has at room temperature a reaction rate $k < 1$ on

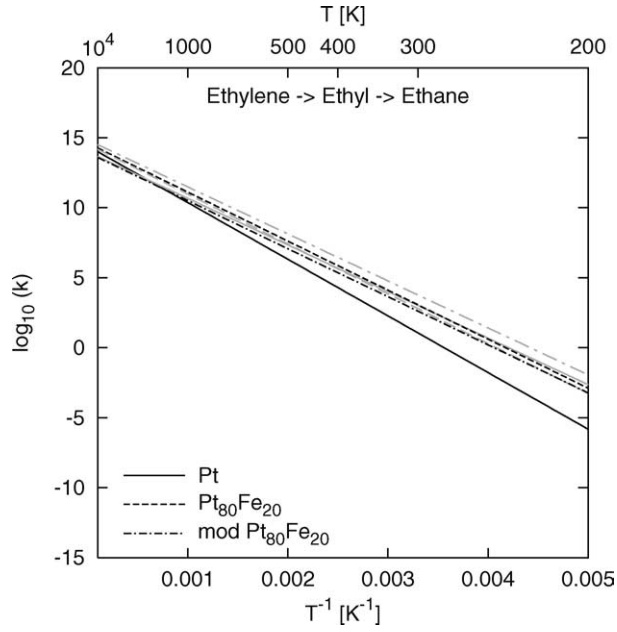

Fig. 8. Logarithm of the reaction rate constants for the hydrogenation of ethylene on different surfaces. Lines for the first and second hydrogenation are black and gray, respectively.

the platinum-covered surfaces and only $k \approx 10$ on the modified surface; this process is therefore extremely unlikely as was already seen from the high reaction barrier.

6. Conclusions

Following the theoretical investigation of the $Pt_{80}Fe_{20}$ (111) surface [36] and the determination of aldehyde chemisorption energies on it [11], we have studied the hydrogenation of C=C and C=O double bonds in ethylene and formaldehyde on pure Pt (111) and $Pt_{80}Fe_{20}$ (111) surfaces as a first step toward the understanding of the experimentally observed selectivity of the alloy surface in hydrogenating α,β-unsaturated aldehydes to unsaturated alcohols. Starting from the adsorption energies of reactants, intermediates, and products, we have identified and characterized transition states for the formation of H–C and H–O bonds and determined the corresponding energy barriers on various sur-

Table 4
Energy barriers and prefactors for the hydrogenation of formaldehyde and ethylene over pure Pt and PtFe alloy surfaces

Path	Surface	$\Delta E_{act}^{(1)}$ (meV)	$\Delta E_{act,zp}^{(1)}$ (meV)	$\nu^{(1)}$ (10^{12} s^{-1})	$\Delta E_{act}^{(2)}$ (meV)	$\Delta E_{act,zp}^{(2)}$ (meV)	$\nu^{(2)}$ (10^{12} s^{-1})
$C_2H_4 \rightarrow C_2H_6$	Pt	803	739	260	660	598	99
$C_2H_4 \rightarrow C_2H_6$	$Pt_{80}Fe_{20}$	695	620	420	706	646	340
$C_2H_4 \rightarrow C_2H_6$	Mod. $Pt_{80}Fe_{20}$	681	616	87	666	593	704
$CH_2O \rightarrow CH_3O \rightarrow CH_3OH$	Pt	391	344	633	142	128	1.6
$CH_2O \rightarrow CH_3O \rightarrow CH_3OH$	$Pt_{80}Fe_{20}$	491	451	9.5	243	211	5.8
$CH_2O \rightarrow CH_3O \rightarrow CH_3OH$	Mod. $Pt_{80}Fe_{20}$	594	503	2700	506	427	46
$CH_2O \rightarrow CH_2OH \rightarrow CH_3OH$	Pt	444	349	24,000	1104	1049	320
$CH_2O \rightarrow CH_2OH \rightarrow CH_3OH$	$Pt_{80}Fe_{20}$	461	413	46	1131	1046	36,000
$CH_2O \rightarrow CH_2OH \rightarrow CH_3OH$	Mod. $Pt_{80}Fe_{20}$	592	505	29	787	712	230

The species to be hydrogenated are initially adsorbed in a di-σ mode.

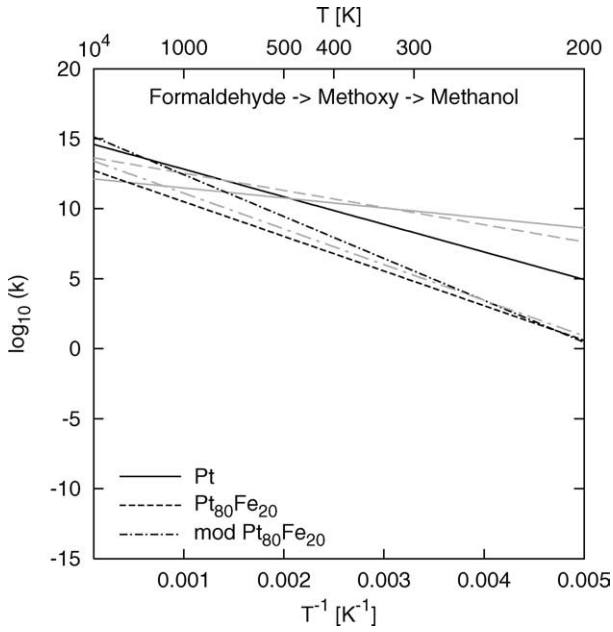

Fig. 9. Logarithm of the reaction rate constants for the hydrogenation of formaldehyde via methoxy on different surfaces. Lines for the first and second hydrogenation are black and gray, respectively.

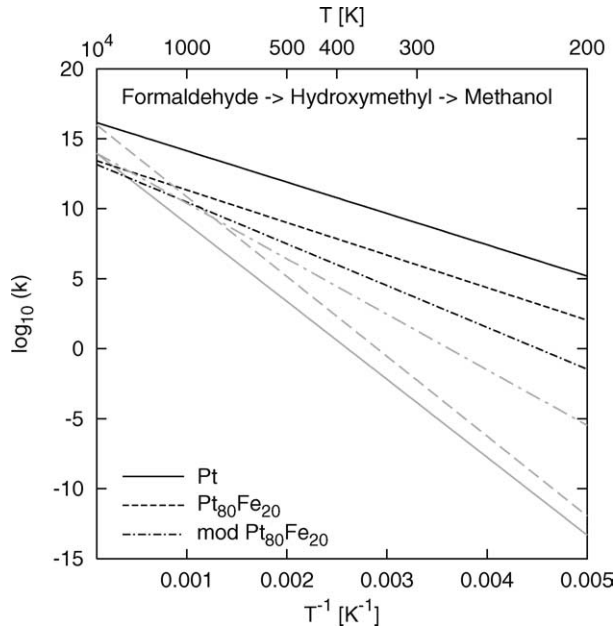

Fig. 10. Logarithm of the reaction rate constants for the hydrogenation of formaldehyde via hydroxymethyl on different surfaces. Lines for the first and second hydrogenation are black and gray, respectively.

faces. Besides the pure Pt (111) surface and a segregated $Pt_{80}Fe_{20}$ (111) surface simulated by a Pt_3Fe bulk terminated by a layer of pure platinum, we have chosen a so-called "modified" $Pt_{80}Fe_{20}$ surface, having a second layer Fe atom interchanged with a surface platinum atom, thereby presenting iron atoms in the surface layer. The local reversal of the surface segregation is driven for formaldehyde, as also demonstrated in our previous study of the adsorption of unsaturated aldehydes, by the strong differences in the adsorbate bonding with Fe and Pt atoms. No such effect is predicted for ethylene.

When hydrogenating ethylene, the local chemical environment of the platinum atoms interacting with the adsorbate does not have a significant influence besides reducing adsorption energies, neither on the reaction geometry nor on the reaction barriers, which are around 700 meV for all hydrogenation steps involved.

In the hydrogenation of formaldehyde, all C–H bond formations are overall endothermic while all O–H bond formations are exothermic. The first bond to be built is equally probable to be either of the two, since the reaction barriers are almost identical. However, the hydroxymethyl intermediate is a very stable species on the surface. If it reacts at all it is more likely to be decomposed into hydrogen and formaldehyde again than to be successively hydrogenated to methanol. The methoxy intermediate, on the other hand, can very easily be further hydrogenated to methanol with an activation energy of only ~ 200 meV on the platinum-covered surfaces and 430 meV (including zero-point corrections) on the modified surface. On the modified surface all barriers are below the adsorption energy of formaldehyde. The determination of reaction rates confirms the conclusions based on the $T = 0$ K results regarding reaction probabilities and rate-determining steps at room temperature.

On the investigation of the hydrogenation reactions we observed a favored coadsorption of hydrogen near Fe–O bonds. Calculations on the coadsorption of unsaturated aldehydes and hydrogen confirmed this situation also for larger adsorbates. The energy gain is around 30 meV, while the coadsorption of hydrogen and another molecule near a Pt surface atom "costs" about 200 meV compared to an individual adsorption of the two species "far away" from each other.

We are now able to suggest an explanation for the selective hydrogenation of α,β-unsaturated aldehydes toward unsaturated alcohols on $Pt_{80}Fe_{20}$ surfaces. These aldehydes adsorb in a flat geometry on the surface, including the interaction of *both* double bonds with the surface. While on the clean surface Pt segregates to the topmost layer, the favored formation of O–Fe bonds changes the segregation profile and almost restores the bulk stoichiometry at the surface. Coadsorbed hydrogen atoms favorably diffuse close to the C=O double bond attached to the surface Fe atom. Not only is the diffusion barrier of hydrogen on platinum surfaces very low, i.e., the atoms are mobile, also the hydrogenation near Fe–O bonds is favored over all other adsorption sites. After the first O–H bond formation the carbon radical at the other end of the former C=O double bond is immediately also hydrogenated, leading to the unsaturated alcohol. The latter is adsorbed in a diσ_{CC} configuration via the remaining double bond. Our previous results [11] suggest that the adsorption energy for prenal is around 0.3 eV, while for allyl alcohol it is around 0.7 eV. The diffusion of a hydrogen atom toward the C=C double bond is associated with an energy cost of about 0.2 eV; the following reaction barrier for the hydrogenation is around 0.7 eV. Consequently, prenal will almost certainly desorb before it can become hydrogenated to isopentyl alcohol, while in the case of allyl alcohol a further hydrogenation to propyl alcohol is more prone to occur.

Summarizing, we have in the last three sections proposed a scenario of a complex catalytic phenomenon from first principles that now awaits experimental verification. The behavior of other platinum-based alloys is very likely to follow a similar pattern. For example, recent work of Nørskov and co-workers [44,45] has investigated the promoting effect of alloying Pt with Sn or Ru on electro-oxidation and hydrogenation reactions. It was emphasized that alloying leads to a surface heterogeneity suppressing the formation of certain adsorbed species while promoting others and thereby improving reaction selectivity. The interplay between selective adsorption and surface structure and composition, however, is a novel aspect of our work.

Acknowledgments

We thank Prof. Philippe Sautet and Dr. Francoise Delbecq for fruitful discussions. R. Hirschl has been supported by the Austrian Science Funds through the Joint Research Project Gas–Surface Interactions (FWF S8106-PHY). The Schrödinger cluster of the Computer Center of the Universität Wien has been used for the numerical work.

References

[1] G.E. Moore, Electronics 38 (1965) 114.
[2] P. Beccat, J.C. Bertolini, Y. Gauthier, J. Massardier, P. Ruiz, J. Catal. 126 (1990) 451.
[3] P. Claus, Top. Catal. 5 (1998) 51.
[4] P. Gallezot, D. Richard, Catal. Rev. Sci. Eng. 40 (1998) 81.
[5] M. English, V.S. Ranade, J.A. Lercher, J. Mol. Catal. A 121 (1997) 69.
[6] T.B.L.W. Marinelli, S. Nabuurs, V. Ponec, J. Catal. 151 (1995) 431.
[7] V. Ponec, Appl. Catal. A 149 (1997) 27.
[8] N. Homs, J. Llorca, P. Ramírez de la Piscina, F. Rodríguez-Reinoso, A. Sepúlveda-Escribano, J. Silvestre-Albero, Phys. Chem. Chem. Phys. 3 (2001) 1782.
[9] C. Mohr, P. Claus, Sci. Progr. 84 (2001) 311.
[10] J. Horiuti, M. Polanyi, Trans. Faraday Soc. 30 (1934) 1164.
[11] R. Hirschl, F. Delbecq, P. Sautet, J. Hafner, J. Catal. 217 (2003) 354.
[12] P. Beccat, Y. Gauthier, R. Baudoing-Savois, J.C. Bertolini, Surf. Sci. 238 (1990) 105.
[13] F. Zaera, T.V.W. Janssens, H. Öfner, Surf. Sci. 368 (1996) 371.
[14] P.S. Cremer, X. Su, Y.R. Shen, G.A. Somorjai, J. Am. Chem. Soc. 118 (1996) 2942.
[15] A.F. Carlsson, R.J. Madix, J. Chem. Phys. 115 (2001) 8074.
[16] M. Neurock, V. Pallassana, R.A. van Santen, J. Am. Chem. Soc. 122 (2000) 1150.
[17] T. Miura, H. Kobayashi, K. Domen, J. Phys. Chem. B 104 (2000) 6809.
[18] K. Aika, H. Sekiya, A. Ozaki, Chem. Lett. 3 (1983) 301.
[19] S.K. Desai, M. Neurock, K. Kourtakis, J. Phys. Chem. B 106 (2002) 2559.
[20] G. Kresse, J. Furthmüller, Phys. Rev. B 54 (1996) 11169.
[21] G. Kresse, J. Hafner, Phys. Rev. B 49 (1994) 14251.
[22] G. Kresse, J. Hafner, Phys. Rev. B 47 (1993) 558.
[23] G. Kresse, J. Furthmüller, Comp. Mater. Sci. 6 (1996) 15.
[24] J.P. Perdew, Y. Wang, Phys. Rev. B 45 (1992) 13244.
[25] H.J. Monkhorst, J.D. Pack, Phys. Rev. B 13 (1976) 5188.
[26] P. Blöchl, Phys. Rev. B 50 (1994) 17.
[27] G. Kresse, D. Joubert, Phys. Rev. B 59 (1999) 1758.
[28] G. Mills, H. Jónsson, Phys. Rev. Lett. 72 (1994) 1124.
[29] G. Mills, H. Jónsson, G.K. Schenter, Surf. Sci. 324 (1995) 305.
[30] G. Henkelmann, B.P. Uberuaga, H. Jónsson, J. Chem. Phys. 113 (2000) 9901.
[31] R.A. van Santen, J.W. Niemantsverdriet, Chemical Kinetics and Catalysis, Plenum, New York, 1995.
[32] A. Eichler, J. Hafner, Chem. Phys. Lett. 343 (2001) 383.
[33] N. Barrett, C. Guillot, J.C. Bertolini, J. Massardier, B.C. Khanra, Surf. Sci. Lett. 260 (1992) L11.
[34] C. Creemers, P. Deurinck, Surf. Interface Anal. 25 (1997) 177.
[35] A.V. Ruban, H.L. Skriver, J.K. Nørskov, Phys. Rev. B 59 (1999) 15990.
[36] R. Hirschl, F. Delbecq, P. Sautet, J. Hafner, Phys. Rev. B 66 (2002) 155438.
[37] V. Ponec, C.G. Bond, Catalysis by Metals and Alloys, Elsevier, New York, 1995.
[38] T.P. Beebe, J.T. Yates, J. Am. Chem. Soc. 108 (1986) 663.
[39] N.M. Abbas, R.J. Madix, Appl. Surf. Sci. 7 (1981) 241.
[40] I. Villegas, M.J. Weaver, J. Chem. Phys. 103 (1995) 2295.
[41] M. Neurock, private communications.
[42] F. Zaera, Langmuir 12 (1996) 88.
[43] A.P. Graham, A. Menzel, J.P. Toennies, J. Chem. Phys. 111 (1999) 1676.
[44] R.W. Watwe, R.D. Cortright, M. Mavrikakis, J.K. Nørskov, J.A. Dumesic, J. Chem. Phys. 114 (2002) 4663.
[45] P. Liu, A. Logadottir, J.K. Nørskov, Electrochim. Acta 48 (2003) 3731.